AD-A150 115 SURFACE FORWARD SCATTERING AND REFLECTION(U) WASHINGTON UNIV SEATTLE APPLIED PHYSICS LAB E I THORSOS MAY 84 APL-UW-7-83 N00024-81-C-6042 1/1

UNCLASSIFIED F/G 20/1 NL

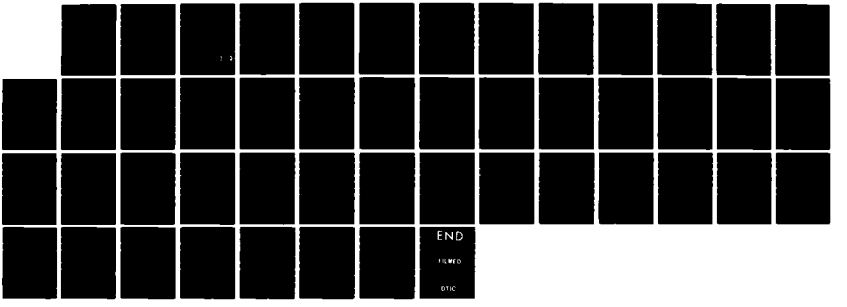

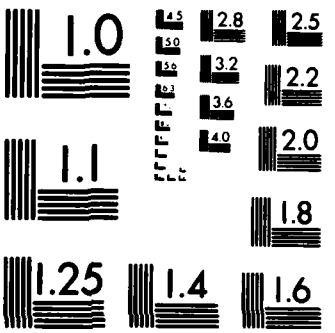

Surface Forward Scattering and Reflection

APL-UW 7-83
May 1984

Contract N00024-81-C-6042

Surface Forward Scattering and Reflection

by

E. I. Thorsos

APL-UW 7-83
May 1984

Applied Physics Laboratory University of Washington
Seattle, Washington 98105

Contract N00024-81-C-6042

ACKNOWLEDGMENTS

This research was conducted under sponsorship of the High Frequency Block Program and managed by the Naval Ocean Research and Development Activity (NORDA) under NAVSEA contract N00024-81-C-6042.

CONTENTS

I. INTRODUCTION

This report discusses high frequency (15-60 kHz) models of surface forward scattering and reflection that are appropriate for use in acoustic simulations based on ray tracing techniques.

Typically, some of the following properties of a pulse after a single surface interaction are needed for modeling purposes: (1) the amplitude as a function of time in or near the specular direction (for example, this gives pulse elongation); (2) the corresponding amplitude statistics; (3) the partitioning into scattered (incoherent) and reflected (coherent) components in the specular direction; and (4) the changes in the frequency spectrum due to the moving surface. At a simpler level, (5) an effective reflection loss may be needed, e.g., for reverberation or one-way propagation simulations. At a more detailed level, (6) two-point statistics at the receiver may be desired. In what follows an attempt will be made to describe models for (1)-(5), but item (6) will not be addressed. With regard to scattering, it will be assumed that the primary interest for simulations lies in representing the scattered signal by an effective reflection loss due to the difficulty of including forward scattering in simulations. Thus, a detailed description of the angular distribution of the scattered intensity near the specular direction will not be given.

The present lack of comprehensive experimental studies of surface forward scattering at high frequencies forces considerable reliance on heuristic arguments, theoretical studies, the use of experimental results at lower frequencies, and the use of laboratory experiments often at even higher frequencies. Important absorption effects of near surface bubbles due to breaking waves must also be taken into account.

II. SCATTERING AND REFLECTION

The terminology here will be to restrict the term "reflection" to the description of the coherent* component of the pressure field that exists after a surface interaction. "Scattering" is associated with the incoherent component. The distinction between reflection and scattering is important because the range dependence of the two components can differ (see Clay[3] for a related discussion). The amplitude statistics and frequency redistribution are also affected by the presence of a reflected component. Reflection can be described by a coherent reflection loss, RL_{coh}:

$$RL_{coh} = -10 \log R \ ,$$

where R is the intensity reflection coefficient of the surface. Forward scattering can be described[5,6] by a scattering strength, S_S (similar to that used for backscattering):

$$S_S = 10 \log \sigma \ ,$$

where σ is the surface scattering cross section per unit solid angle per unit surface area, and is dimensionless.

Fortunately, the complexities of using a scattering strength or scattering cross section can be avoided in some cases. Theoretical treatments of forward scattering using the Kirchhoff approximation in the Fresnel limit have shown[7-9] that when the transmitting and receiving beam widths are sufficiently wide (and the pulse length sufficiently long) to include the entire "active" scattering region then the total intensity after a single surface bounce, excluding the direct path contribution and neglecting absorption due to bubbles, is given by

$$I_{total} = I_{coherent} + I_{incoherent} = \frac{I_t A_0}{(\tau_1 + \tau_2)^2} \ , \qquad (1)$$

---

* The term coherence is used here in the usual sense[1-4]. The coherent component of the outgoing acoustic field has a definite phase relationship with the ingoing or incident wave; it is given by taking an average over an ensemble of surfaces or, equivalently, over an ensemble of pings. The incoherent part fluctuates from ping to ping.

where

I_t is the transmitted intensity at unit distance,

r_1 and r_2 are the specular slant ranges from the transmitter and receiver to the surface,

A_0 is a unit area.

This result can be understood as a consequence of energy conservation when the beam widths are large compared to the angular broadening due to scattering. Equation (1) is valid for large or small surface roughness and indicates that for many conditions the surface interaction can be described by a 0 dB loss for total intensity when attenuation due to near surface bubbles can be neglected. A discussion of the conditions when Eq. (1) is expected to apply will be given subsequently.

Note that Eq. (1) would be the result for a cw transmitting source. For a finite pulse width, the time dependence of the received intensity requires specification. Both this time dependence and the frequency spreading effects are conveniently described by a scattering function.[10,11] We will avoid these more formal developments here and simply write the received intensity as

$$I_{received}(t) = I_{total}(t)\alpha_b \quad , \tag{2}$$

where

$I_{total}(t)$ is the total time dependent intensity (coherent plus incoherent) following the surface interaction, neglecting absorption,

α_b is an absorption factor due to bubbles.

Then, separately, the frequency spreading due to the surface interaction will be specified. In Eq. (2) we are making the assumption that the forward scattered signal is dominated by the part that penetrates the bubble layer, is attenuated in the process, and scatters from the surface.

The separation of the total intensity into coherent and incoherent intensities is most meaningful when the size of the Fresnel zones on the surface is large compared to the spatial correlation length of the surface roughness. This condition should be satisfied for wind driven waves.[12] In cases of swell with no wind, however, this condition may not be satisfied. Surface scattering in this latter case has been described in terms of focusing or defocusing from curved surfaces,[13,14] but will not be considered here.

III. SURFACE ROUGHNESS

The surface roughness parameter* is given by[15]

$$\chi = \frac{2\pi h \left[\sin \theta_1 + \sin \theta_2\right]}{\lambda} , \tag{3}$$

where

h = rms surface waveheight,
λ = acoustic wavelength,
θ_1 = incident grazing angle,
θ_2 = outgoing grazing angle.

The roughness parameter is useful for classification of roughness regimes. For $\chi \lesssim 0.5$, the surface interaction is principally a reflection; for $\chi \gtrsim 2.0$, scattering dominates. At intermediate values of χ, the two components can be comparable. By taking χ into account, experimental data obtained outside the frequency range of primary interest (15-60 kHz) can be used to gain insight when corresponding data over 15-60 kHz are lacking. The rms waveheight, h, which results in a roughness parameter of 1, i.e., the transitional h, is shown in Figure 1 as a function of frequency for grazing angles of 5° and 10° (assuming $\theta_1 = \theta_2$ and c = 1500 m/s). If h is large compared to about 0.05 m (2 in.), scattering can be considered dominant. The rms waveheight h can be related to the significant waveheight $H_{\frac{1}{3}}$ (the average peak-to-trough height of the $\frac{1}{3}$ largest waves) by $H_{\frac{1}{3}} = 4.0h$, if a Pierson-Moskowitz[16,17] surface wave spectrum is assumed. Since the open ocean typically has larger significant waveheights than 0.2 m (0.7 ft), coherent reflection tends not to be the important mode of surface interaction in the open ocean at high frequencies. Coherent reflection loss will be considered in the next section, however, since fetch limited conditions with low surface roughness can be of interest.

* The symbols g or $\sqrt{g}$ are also commonly used instead of χ.

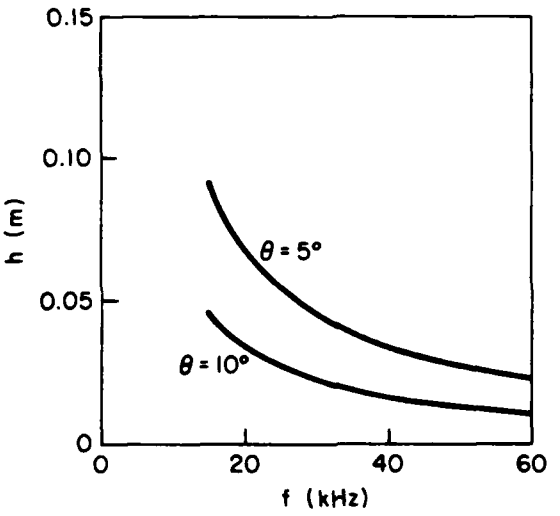

Figure 1. The rms waveheight, h, vs the frequency, f, which results in a surface roughness parameter of $\chi = 1$ for specular grazing angles, θ, of 5° and 10°. In the Kirchhoff approximation, $\chi = 1$ yields an intensity reflection coefficient of e^{-1} (see Section IV).

IV. COHERENT REFLECTION LOSS

If the total intensity following a surface bounce is divided into coherent and incoherent intensities, then the reflection loss RL_{coh} due to the surface interaction and associated with the coherent part alone may be of interest. Whenever the coherent intensity is significant, bubble losses can be neglected.

The coherent intensity reflection coefficient given theoretically in the Kirchhoff approximation, assuming a Gaussian distribution of surface heights, is[1,2,4]

$$R = e^{-\chi^2} , \tag{4}$$

where χ is the roughness parameter with $\theta_1 = \theta_2 \equiv \theta$. Measurements[18-20] have shown Eq. (4) to be a good approximation for artificially constructed surfaces when $\chi \lesssim 1$. Laboratory experiments[21] have further verified the single scatter Kirchhoff prediction for reflection losses up to about $\chi = 2$. In this work the measured surface height distribution, which differed from a Gaussian form, was used for obtaining the Kirchhoff prediction. The reflection loss was predicted correctly up to about 20 dB, which gives additional support for the theoretical assumptions underlying Eq. (4). For large χ the reflected component becomes very small compared to the scattered component and difficult to measure. Since measurements[22] have shown the Gaussian height distribution to be a reasonable approximation for the sea surface, Eq. (4) can be expected to apply approximately to sea surface scattering.

When only the coherent or reflected intensity is being computed following a surface bounce, rather than the total intensity, we recommend use of Eq. (4), which leads to a reflection loss of

$$RL_{coh}\ (\text{dB}) = 305 f^2 h^2 \sin^2\theta , \tag{5}$$

with f in kHz, h in m, and where $c = 1500$ m/s has been assumed. The reflected (coherent) pulse shows no pulse elongation, no frequency broadening or shifting,[23] no ping-to-ping fluctuation (by definition), and is restricted to the specular condition $\theta_1 = \theta_2$.

An important caveat must be placed on Eq. (5) for low grazing angles. Direct experimental verification is not available for the very low grazing angles (0°-5°) often encountered in simulations. Also, the theoretical result Eq. (4) is known to be

unreliable at low grazing angles because shadowing and multiple scattering have not been included, and the Kirchhoff approximation breaks down as well.[24,25] Thus, when $\chi \gtrsim 0.5$, and $\theta < \gamma_0$, where γ_0 is the rms surface slope angle (typically about 8°; see next section), Eq. (5) has the greatest uncertainty. For $\chi \lesssim 0.5$, more accurate perturbation theory[26-30] can be used. Kuperman[31] has computed reflection losses in this way at 750 Hz and 1500 Hz using the Pierson–Moskowitz spectrum, and finds higher losses than given by Eq. (5). However, perturbation theory does show that the reflection loss vanishes as $\theta \to 0$ in agreement with Eq. (5).

V. INCOHERENT SCATTERING

We now turn to a more detailed description of the scattered intensity. First some qualitative features of high frequency forward scattering will be introduced based on heuristic arguments. This will motivate an estimate of the beam width necessary for the use of Eq. (1) and its time dependent analogue.

A. Implications of Beam Width

The angular distribution of the scattered intensity can be estimated using the high frequency limit, i.e., by using a "facet reflection" model. Evidence that such a model has approximate validity for high frequency forward scattering is given in Appendix A.

In the high frequency limit, the scattered field is determined by the surface slope distribution. As discussed in Appendix A, an effective rms slope angle (γ_0) of about 8° is representative of the ocean surface when the wind speed $U \gtrsim 5$ m/s. This implies that an incident plane wave with grazing angle $\theta_i > 2\gamma_0$ will have an in-plane* scattered intensity distribution extending roughly over the scattered grazing angles $\theta_s = \theta_i \pm 2\gamma_0$, or typically with a spread of about $4\gamma_0 \cong 30°$-$35°$. However, for $\theta_i < \gamma_0$, the angular extent of the scattered intensity will be reduced. For $\theta_i < \gamma_0$ the scattered grazing angle θ_s is bounded by 0° and roughly $\theta_i + 2\gamma_0$, which implies that the scattered vertical "beam" width saturates at about $2\gamma_0 \sim 16°$ as θ_i becomes very small ($\theta_i \ll \gamma_0$). For $\gamma_0 < \theta_i < 2\gamma_0$, the width is roughly $\theta_i + 2\gamma_0$. These estimates are consistent with APL data.[32,33]

If the widths of the transmitting and receiving beams are greater (ideally much greater) than the angular width of the scattered intensity, then we expect Eq. (1) to apply. Thus, in typical propagation and reverberation conditions where $\theta_i \lesssim 10°$, vertical beam widths of 20°-25° are marginally sufficient. Multiple surface bounces will induce further broadening of the scattered angular distribution, and under these conditions broader beam widths may be needed for (1) to apply.

For vertical beam widths narrow compared to the angular width of the scattered intensity, the intensity loss should exceed the 0 dB value given by Eq. (1), but estimates of this effect will not be considered.

---

* For in-plane scattering, the incident and scattered rays are in the same vertical plane.

Scattering out-of-plane, i.e., involving a change in azimuthal angle, is typically confined to much smaller angular widths. For example, with equal source and receiver depths and equal incident and scattered grazing angles, it can be shown that the incident grazing angle, θ_i, the change in azimuthal angle, φ, and the corresponding surface slope angle, γ, are related by

$$\sin(\varphi/2) = \tan\theta_i \tan\gamma \ . \tag{6}$$

If γ is set to 8° (the typical rms value) and if $\theta_i = 10°$, then Eq. (6) yields $\varphi = 2.8°$. In this case, the azimuthal width of the scattered intensity would be estimated at about 6°. For small grazing angles ($\theta_i \lesssim 10°$), therefore, horizontal (azimuthal) transmitting and receiving beam widths are usually sufficiently large so as not to affect the use of Eq. (1).

Experimental support for Eq. (1) is shown in the results of Nichols and Senko,[34] who used essentially omnidirectional sources and receivers* and found that the received intensity was independent of χ over the range of 0.3 to about 9, i.e., independent of χ from the reflection regime into the scattering regime. These measurements were at low frequencies (400-1500 Hz), where absorption due to bubbles can be neglected, and waveheights were up to 9 m (30 ft).

* The pulse widths were also long compared to the pulse elongation time estimates to be discussed later

B. Effective Reflection Loss for Forward Scattering in Reverberation Simulations

In reverberation or total backscattering, ray paths involving surface bounces contribute to the reverberation level, particularly in shallow water. These surface bounces involve surface forward scattering, possibly reflection, and absorption due to near surface bubbles. In general, surface forward scattering will cause pulse elongation in the surface bounce signal.

For reverberation simulations, the pulse elongation due to forward scattering is often unimportant; only the energy or $\int I_{total}(t)dt$ is of significance*. This will be true whenever the time scale over which the reverberation level changes is long compared to the time interval over which the pulse is elongated (see SectionV.C). For such a case, the modeling of surface forward scattering can be simplified considerably. To see how this occurs, first note that a 0 dB intensity loss would be implied by Eq. (1) for cw transmission, assuming the beam widths are sufficiently broad, as discussed in the previous section. Added to this would be any attenuation due to bubbles (Section VI). For a very short pulse width, however, the peak scattered intensity may not reach the cw value, i.e., the important or active scattering regions on the surface may not all contribute simultaneously. Even so, if Eq. (1) is to hold for a long pulse, then it follows that for a short pulse there will be no energy loss at a receiver other than spreading loss as in Eq. (1)**. This justifies the use of a 0 dB effective reflection loss and no pulse elongation for modeling surface forward scattering in reverberation simulations, whenever the time scale over which reverberation changes is long compared to the time interval over which the pulse is elongated. This should be an adequate model for application to boundary and volume reverberation, for example. The final result is that the surface bounce can often be modeled with a reflection loss given entirely by the "surface bubble loss" (SBL) given by Eq. (15) in Section VI.

These arguments have some experimental support. Adlington[35] reported 0 dB (± 3 dB) forward scattering energy losses for short pulse explosive charge data. In this work 0.4 kHz ≤ f ≤ 6.4 kHz and 10° ≤ θ ≤ 55°. No dependence on wind speed was

---

* It is sufficient to take the time interval of integration here to begin at the time of specular path arrival and to extend for a pulse length plus several times the characteristic elongation time T, which is defined in Section V.C.

** This can be seen by viewing a long pulse as a sequence of adjacent short pulses. Superposition of the scattered intensities for the sequence of short pulses will yield Eq. (1) only if each short pulse shows no energy loss at a receiver due to surface scattering.

noted over the range of 3-10 m/s (5-20 kn). Also, recent high frequency reverberation simulations at APL[36,37] for low sea state conditions have obtained the best fit to measured reverberation using a 0 dB effective surface reflection loss model. For all these cases, no significant losses due to bubbles would be expected.

A potential difficulty with using the 0 dB loss model of surface scattering in simulations should also be noted. In the previous section it was estimated that when $\theta_i \ll \gamma_0$ the scattered intensity would be distributed over the range of scattered angles θ_s from 0° to $2\gamma_0 \cong 16°$ for typical surface conditions. In other words, the average scattered angle is not equal to the angle of incidence. Usually in simulations all the scattered energy would instead be assigned $\theta_s = \theta_i$, i.e, scattering would be treated as specular reflection. This difference will cause the simulation rays to have fewer surface and bottom bounces per unit range than would actually occur, an effect of particular significance in shallow water environments. In addition, bottom reflection losses at very low grazing angles will be used when higher losses due to the higher scattered angles are actually appropriate. This coupling between surface and bottom interactions was discussed by Marsh and Schulkin[38] in the context of semiempirical expressions for shallow water transmission loss. Apparently, procedures for using the results of Ref. 38 in ray based simulations have not been developed. One plausible estimate on the simulation uncertainty could be obtained by comparing the standard $\theta_s = \theta_i$ result with an alternative model with θ_s constrained to γ_0 whenever $\theta_i < \gamma_0$. As discussed in Appendix A, we would estimate γ_0 from the wind speed U (in m/s) at a 10 m height as follows:

$$\tan^2 \gamma_0 = 4.6 \times 10^{-3} \ln(2.1U^2) \quad . \qquad U > 1\,\text{m/s} \qquad (7)$$

C. Time Dependent Intensity After Forward Scattering

For one-way propagation with surface bounces, the time dependence or pulse elongation of the scattered signal is of interest. Similarly, in applications such as the simulation of target returns with high time resolution pulses, it may be necessary to account for the pulse elongation effect of the surface interaction. This aspect of surface scattering is difficult to treat, since it depends on the geometry of the scattering event. The theoretical work of McDonald and coworkers[9,11,39-41] will be taken as a guide in formulating an expression for the time dependent intensity. In general for a single surface bounce path, both reflected and scattered signals will be observed during the first part of the received signal with a duration equal to the transmitted pulse length, while subsequently only the scattered signal will be present. The surface roughness will be assumed large ($\chi \gtrsim 2$), however, since this

limit covers most cases of practical interest at high frequencies. The reflected component can therefore be neglected and only incoherent scattering must be treated. The beam widths are assumed sufficiently broad for Eq. (1) to apply for cw transmission, but the topic here is the buildup and decay of the scattered intensity for finite pulse widths. The intensity modeled will correspond to that experimentally obtained from an average over many pings.

Consider first a single surface bounce with incident and scattered slant ranges along the specular path of r_1 and r_2 as shown in Figure 2a. Using the results of Refs. 11 and 39, we find in the high frequency limit (large roughness) and for Gaussian surface statistics that the time dependent intensity scattered from the surface with the direct path excluded can be written

$$I_s(t) = \int_{-\infty}^{\infty} H(t,t')I_t(t')dt' \ , \tag{8}$$

where $I_s(t)$ is the time dependent analogue of $I_{incoherent}$ in Eq. (1), $I_t(t)$ is the transmitted intensity at unit distance, and $H(t,t')$ is an intensity impulse response function of the surface given by*

$$H(t,t') = \frac{A_o}{(r_1+r_2)^2} \frac{\Theta(t-t'-t_s)}{\left[\pi T(t-t'-t_s)\right]^{\frac{1}{2}}} e^{-(t-t'-t_s)/T} \ . \tag{9}$$

In Eq. (9),

A_0 is a unit area,

T is a time related to the time scale of pulse elongation and is defined later,

t_s is the specular path travel time,

$t_s = (r_1 + r_2)/c$, with c the speed of sound,

Θ is the unit step function, i.e.,

$\Theta(t) = 0$ for $t<0$,

$\Theta(t) = 1$ for $t>0$.

It is straightforward to show from Eq. (8) and Eq. (9) that

* Eq. (9) must be modified to apply at angles near vertical incidence.

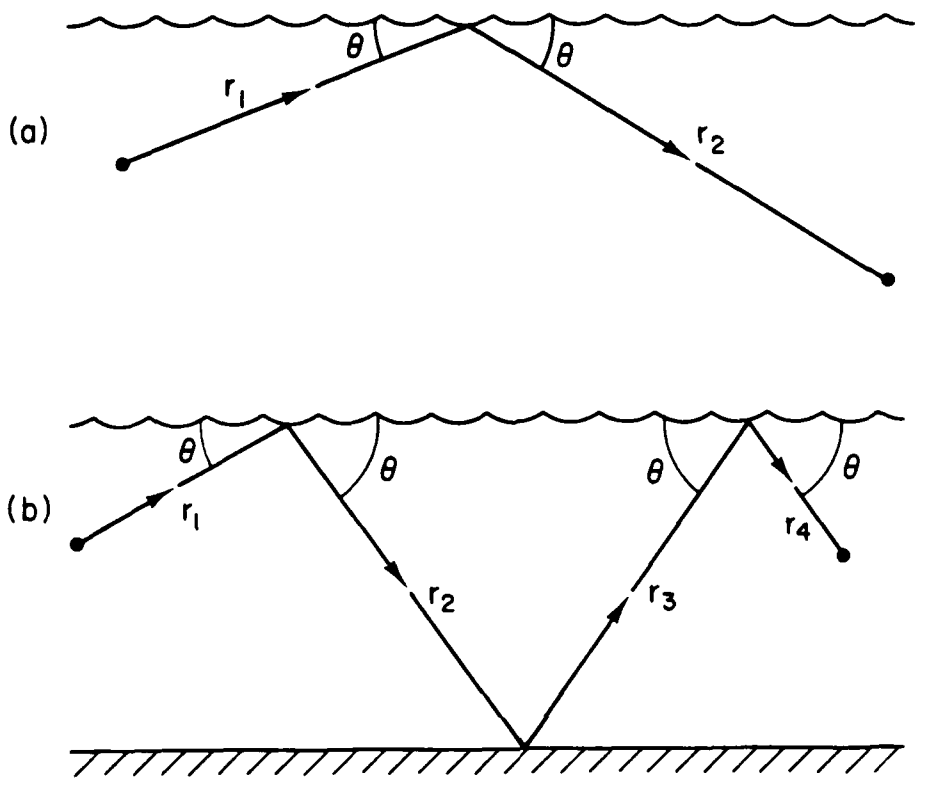

Figure 2. Specular rays for (a) single surface bounce and (b) surface-bottom-surface bounce paths.

$$\int_{-\infty}^{\infty} I_s(t)dt = \frac{A_0}{(\tau_1+\tau_2)^2} \int_{-\infty}^{\infty} I_t(t')dt' \ .$$

Thus, zero energy loss at the surface is insured for all pulse lengths. In particular, for a rectangular transmitted pulse of pulse length τ_0, i.e.,

$$I_t(t) = \begin{cases} 0 & t < 0 \\ I_t \ , & 0 < t < \tau_0 \\ 0 & t > \tau_0 \end{cases} \tag{10}$$

we have

$$\int_{-\infty}^{\infty} I_s(t)dt = \int_{t_s}^{\infty} I_s(t)dt = \frac{I_t \tau_0 A_0}{(\tau_1+\tau_2)^2} \ . \tag{11}$$

For the rectangular pulse of Eq. (10), the explicit form for the scattered intensity from Eq. (8) and Eq. (9) is

$$I_s(\tau) = \frac{I_t A_0}{(\tau_1+\tau_2)^2} \begin{cases} 0 & \tau \leq 0 \\ \Phi\left[\sqrt{\tau/T}\right] & 0 \leq \tau \leq \tau_0 \\ \Phi\left[\sqrt{\tau/T}\right] - \Phi\left[\sqrt{(\tau-\tau_0)/T}\right] & \tau \geq \tau_0 \end{cases} \tag{12}$$

where $\tau = t - t_s$, and where

$$\Phi(x) = \frac{1}{\sqrt{\pi}} \int_0^{x^2} \frac{e^{-t}\,dt}{\sqrt{t}} = \frac{2}{\sqrt{\pi}} \int_0^{x} e^{-t^2}\,dt$$

is the probability integral[42] (error function). T can be viewed as a characteristic elongation time, since $I_s(\tau)$ given by Eq. (12) decays exponentially with a characteristic time T when $(\tau - \tau_0) / T \gg 1$. Near the time of maximum intensity, however, the time scale of intensity rise and fall is closer to $T/2$.

The time T is given by

$$T = \left[\frac{2\tau_1\tau_2}{\tau_1 + \tau_2} \frac{\tan^2\gamma_0}{c} \right] \left[1 - e^{-\theta/\gamma_0} \right] . \tag{13}$$

In Eq. (13), the first factor is the expression for T that follows from Refs. 11 and 39, where the grazing angle θ is implicitly assumed to be large compared to the rms slope angle γ_0. Results of a simple facet reflection model for arbitrary θ/γ_0 can be incorporated to a good approximation with the second factor, and thus we adopt Eq. (13) for T. As an example, consider $\tau_1 = \tau_2$, with $\theta = 10°$, $\gamma_0 = 8°$, and $c = 1500$ m/s. From Eq. (13),

$$T = 9.4\tau_1 = 4.6R ,$$

where R is the horizontal range, T is in ms, and τ_1 and R are in km. For R = 1 km, T = 4.6 ms; for R = 200 m, T = 0.9 ms.

Almost all APL surface scattering data have been obtained with narrow beams and thus do not provide direct experimental tests of Eq. (12). However, one recently obtained data set[43] with good signal-to-noise using an omnidirectional receiver and a broad beam transmitter is marginally suitable for comparison. The experimental conditions were as follows:

Location: Dabob Bay (~ 8 km west of Bangor, WA)
Wind speed: U = 4.1 m/s (8 kn)
Roughness parameter: χ = 1.22
Pulse length: τ_0 = 1 ms
Specular grazing angle: θ = 11.7°
Horizontal range: R = 1.26 km
Transducer depths: 114 m and 146 m
Vertical beam width of transmitter: 44°.

The large roughness condition is not fully met, and this limits somewhat the suitability of the data set. Since χ is not above 2, coherent reflection will be taken into account by writing

$$I_{total}(\tau) = \begin{cases} \dfrac{I_t A_0}{(\tau_1 + \tau_2)^2} e^{-\chi^2} + \left[1 - e^{-\chi^2} \right] I_s(\tau) & 0 \leq \tau \leq \tau_0 \\ \left[1 - e^{-\chi^2} \right] I_s(\tau) & \tau \geq \tau_0 \end{cases} \tag{14}$$

with $I_s(\tau)$ given by Eq. (12). From Eq. (7), $\gamma_0 \cong 7.3°$, and Eq. (13) yields $T = 5.53$ ms. The time dependent intensity from Eq. (14) is compared with the result of a 100-ping average of the data in Figure 3. For this comparison, the maximum intensity from Eq. (14) was made to coincide with the experimental maximum by appropriate shifts in the level and time axes. For this case, the time dependence of the intensity is in reasonable agreement with the measurement, but further experimental verification is needed.

The single surface interaction treatment can be generalized to multiple bounces following Tuteur and McDonald,[11] but there is no direct experimental support. Consider the surface-bottom-surface bounce path shown in Figure 2b. The bottom bounce will be assumed a perfect reflection to simplify the discussion. For a rectangular transmitted pulse, the time dependent intensity is given by Eq. (12) with

$$\tau_1 + \tau_2 \rightarrow \tau_1 + \tau_2 + \tau_3 + \tau_4 \ ,$$

and

$$T = T_1 + T_2 \ .$$

The time T_1 is found from Eq. (13) with

$$\left[\frac{\tau_1\tau_2}{\tau_1 + \tau_2}\right] \rightarrow \frac{\tau_1(\tau_2 + \tau_3 + \tau_4)}{\tau_1 + (\tau_2 + \tau_3 + \tau_4)} \ ,$$

i.e., by effectively considering the second surface bounce to be a perfect reflection. Similarly, T_2 is found from Eq. (13) with

$$\left[\frac{\tau_1\tau_2}{\tau_1 + \tau_2}\right] \rightarrow \frac{(\tau_1 + \tau_2 + \tau_3)\tau_4}{(\tau_1 + \tau_2 + \tau_3) + \tau_4} \ .$$

Generalization to any number of bounces is straightforward.

In terms of even more approximate forms, a 0 dB effective reflection loss with no pulse elongation is adequate if total energy is the primary interest. If only peak intensity is relevant, an intensity reflection coefficient

$$R = \Phi\left[\sqrt{\tau_0 / T}\right] ,$$

with a scattered pulse length τ_0 / R could be used. In this approximation, Eq. (12) becomes

$$I_s(\tau) = \frac{I_t A_0}{(r_1 + r_2)^2} \begin{cases} R & 0 \leq \tau \leq \tau_0 / R \\ 0 & \tau > \tau_0 / R \end{cases} .$$

It must be emphasized that further experimental verification is needed for the results of this section. Isovelocity conditions have been implicitly assumed and the generalization to the nonisovelocity case has not been treated. Uncertainties exist in the small grazing angle limit, and remarks in Section V.B regarding estimates of simulation uncertainty could be applied here as well for cases with multiple bounces. It is hoped that this discussion will at least supply guidance on the expected form of the time dependent intensity in surface forward scattering.

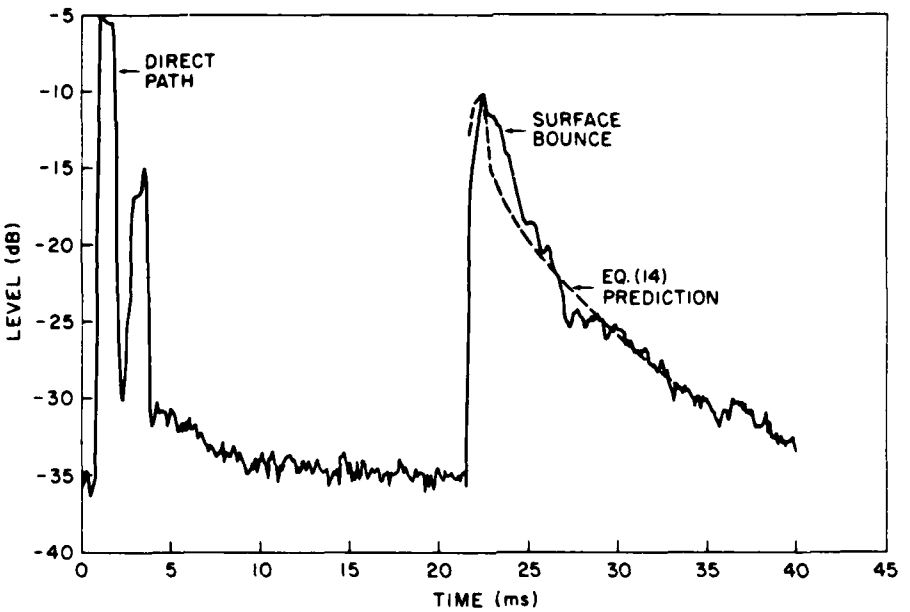

Figure 3. Envelope amplitude time history showing direct and surface bounce signals together with the prediction from Eq. (14). The pulse following immediately after the main direct path is presumed to be an additional direct path and to not contribute to the surface bounce. The zero of time is shifted from that in the text.

VI. ABSORPTION DUE TO NEAR SURFACE BUBBLES

The significance of absorption due to bubbles in surface sound-channel propagation has been stressed by Schulkin,[44] and more recently by Novarini and Bruno,[45] but otherwise this aspect of surface forward scattering has received little attention. Figure 4 shows in-plane forward scattering strengths[33] at a wind speed of 20 m/s where high absorption from bubbles is strongly suspected. The model curve is based on the high frequency limit (see Appendix A for a description of the model and for a definition of the slope angle γ); we would expect the curve tc at least be in the vicinity of the data if no absorption from bubbles took place. Reasonable agreement with this model is found for low wind speed as shown in Appendix A. We take the large difference between the model prediction and the measurement to be indirect evidence of high absorption due to bubbles in surface forward scattering at a wind speed of 20 m/s.

Unfortunately, the modeling of this attenuation has large uncertainties. The data base* on bubble populations must be considered insufficient for developing empirical forms for bubble size and depth distributions as a function of wind speed. In addition, studies of bubble distributions by Thorpe[47] show complicated spatial structure, which indicates that the relationship between the average bubble distributions and absorption in forward scattering may not be straightforward. Therefore, the "surface bubble loss" model developed here has the potential for large error. The surface bubble loss (SBL) is related to α_b in Eq. (2) by SBL (dB) = -10 log α_b.

The choices made in arriving at a bubble loss model are outlined in Appendix B. The loss estimates are based on bubble distributions measured by Johnson and Cooke[48] and Kolovayev.[49] The final result is

$$\mathrm{SBL(dB)} = \left[\frac{1.12 \times 10^{-7}}{\sin\theta}\right] U^{6.5} f^{0.5}, \qquad 15\mathrm{kHz} \leq f \leq 24\mathrm{kHz} \qquad (15a)$$

$$\mathrm{SBL(dB)} = \left[\frac{9.53 \times 10^{-10}}{\sin\theta}\right] U^{6.5} f^{2.0}, \qquad 24\mathrm{kHz} \leq f \leq 48\mathrm{kHz} \qquad (15b)$$

for grazing angle θ, wind speed U in m/s at a 10 m height, and frequency f in kHz.

* Bubble measurement techniques and results have been summarized by Wu.[46]

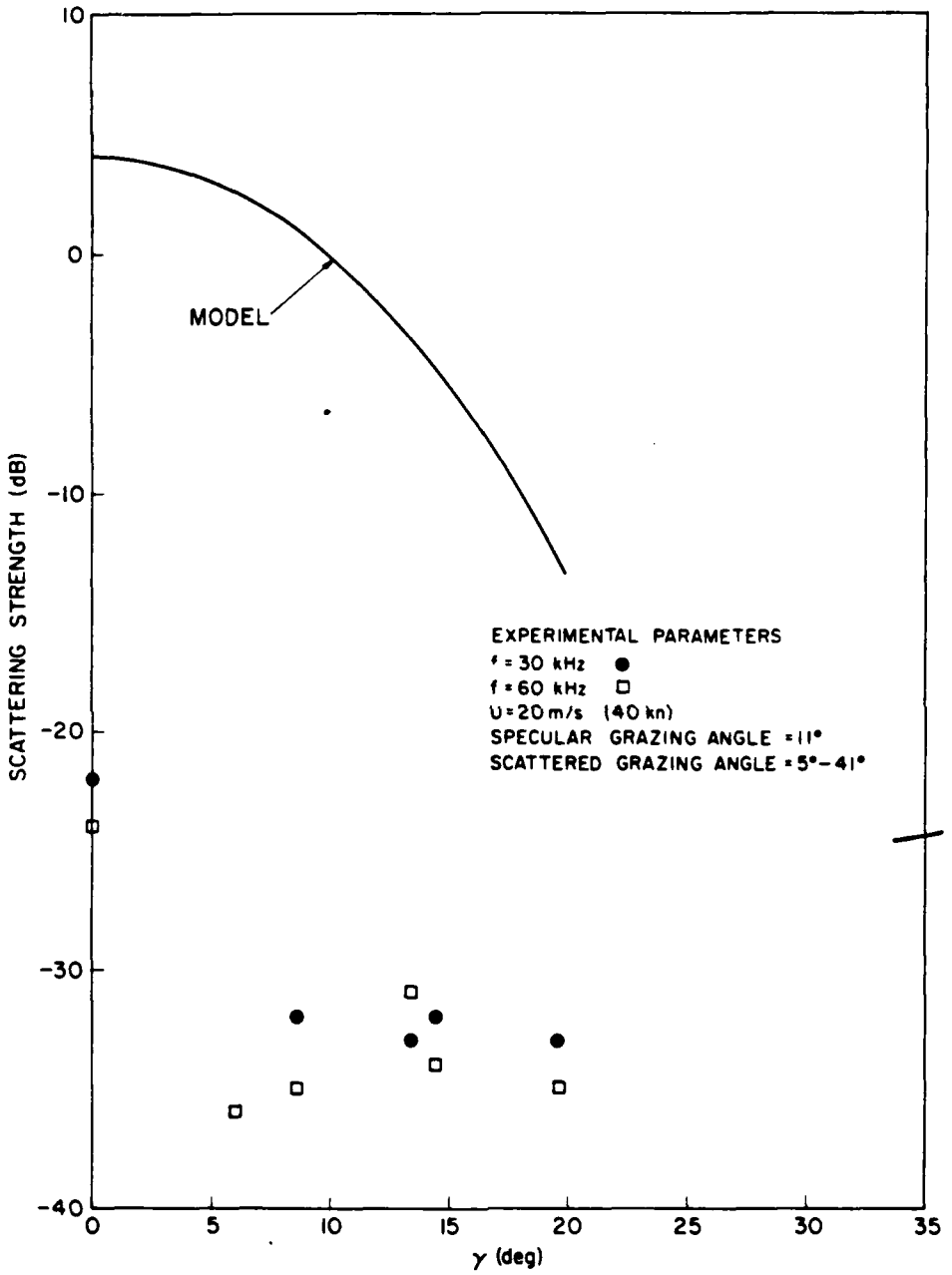

Figure 4. Measured in-plane surface forward scattering strengths at high wind speed compared with a model based on the high frequency limit. See Appendix A for a description of the model and for a definition of the slope angle γ.

The bubble data do not support a sharp break in the frequency dependence at 24 kHz, but there does appear to be a gradual change to a slower frequency dependence at lower frequencies.

It is interesting to compare Eq. (15a) to AMOS results[44] for intensity loss, which Schulkin suggested were due at least in part to bubble absorption. Starting with Eq. (15a), we use the Pierson–Moskowitz spectrum[17] to convert wind speed to rms waveheight h in m $\left[U = 17.7h^{\frac{1}{2}}\right]$; θ is estimated[50] to be 2°–3°, so we set $\theta = 2.5°$; and converting to the units of Ref. 44 we find

$$\text{SBL(dB)} = 1.31h^{2.75}(hf)^{0.5} , \qquad \begin{bmatrix} h \text{ in ft} \\ f \text{ in kHz} \end{bmatrix}$$

while AMOS data imply

$$\text{Loss (dB)} = 1.64(hf)^{0.5} . \qquad \begin{bmatrix} h \text{ in ft} \\ f \text{ in kHz} \end{bmatrix}$$

The waveheight dependence is very different, but at rms waveheights of about 1 ft (which corresponds to reasonably typical wind speeds of about 8 m/s ≅ 15 kn), the losses are similar in magnitude.

The surface bubble loss is a very rapid function of wind speed in the model given by Eq. (15). Figure 5 shows the SBL just at the onset of significant loss. An appropriate surface scattering data base, however, is simply not available at present for verifying the validity of these predictions. For wind speeds above 12 m/s the SBL predicted by Eq. (15) for low grazing angles ($\theta < 10°$) becomes infinite for all practical purposes. A low level scattered signal from the bubble layer will remain, but it is difficult to incorporate this effect correctly in an attenuated effective reflection loss model. A rough estimate based on scattering from bubbles (see Appendix B) indicates that the absorption loss would be bounded at about 30 dB due to scattering. However, such an estimate is uncertain because of dependence on the pulse length and beam widths. Until better information becomes available, we recommend simply using a maximum attenuation of 30 dB whenever Eq. (15) would give an SBL > 30 dB.

Present modeling of surface bubble losses must be considered very uncertain. The possibility of wind gusts and differences in the mean wind speed variation with height near the surface produce uncertainties in relating the wind speed at 10 m to bubble distributions. Further, the likely occurrence of horizontal variations in the near surface bubble distributions will yield uncertainties in relating average bubble distributions to absorption in surface forward scattering. The surface bubble loss in

the 6-8 m/s wind speed range is especially uncertain, because this is near the onset of significant loss and the predicted variation with wind speed is rapid.

One further point should be noted. Because of their rapid falloff with depth, the bubble distributions measured by Johnson and Cooke and by Kolovayev were almost certainly produced by breaking waves at the surface. Medwin[51,52] has measured bubble distributions in Monterey Bay, which apparently are of biological origin and thus are not directly related to the wind speed. These bubbles are of sufficient density to be an important absorption mechanism also, but are not included in the model discussed here.

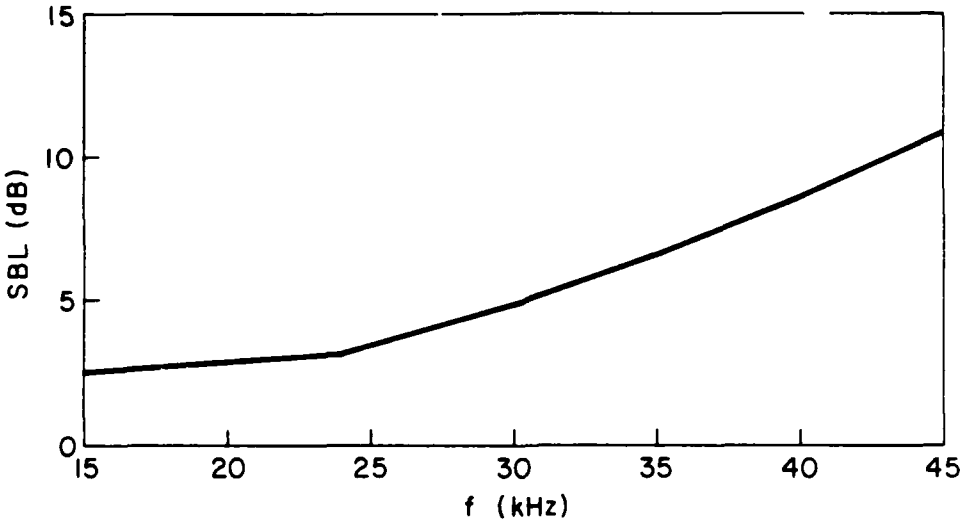

Figure 5. Surface bubble loss (SBL) vs frequency from Eq. (15) for a wind speed of 7.5 m/s and a 5° grazing angle.

VII. FREQUENCY SPREADING

The spectral properties of surface forward scattering have generally been studied with low to moderate surface roughness at lower acoustic frequencies than of direct interest here. From this experimental work[53-60] and other theoretical analyses,[61-68] the following picture has emerged: At low roughness ($\chi \lesssim 1$) the surface bounce signal* is made up of a reflected component, with the same frequency content as the incident pulse, and of a scattered component forming frequency sidebands above and below the incident center frequency. The sidebands are linearly related to the surface wave spectrum and effectively map out this spectrum. The sideband maxima are displaced from the original center frequency by approximately the frequency of the peak of the surface wave spectrum, and the magnitude of the sidebands becomes comparable to the reflected component as χ approaches 1. (See in particular the work of Roderick and Cron.[53])

As the surface roughness increases beyond 1, the scattered spectrum evolves into a Gaussian form, the width becoming large compared to the frequency of the surface wave spectral peak, but still small compared to the corresponding spectral width for backscattering. McDonald and Schultheiss[63] have shown with theoretical studies that the asymptotic Gaussian form is a good approximation to the scattered frequency spectrum when χ reaches 2.5.

Swarts and Eggen[65] have computed** the width of the Gaussian frequency distribution as a function of wind speed U assuming a Pierson–Moskowitz surface wave spectrum. Converting their result to the width of the half power points Δf_{3dB} leads to

$$\Delta f_{3dB}(\text{Hz}) = 0.128 U f \sin\theta \ , \tag{16a}$$

---

* The incident pulse is assumed here to be a narrowband signal.

** The authors used the Kirchhoff approximation and also invoke the Fraunhofer approximation.

with U in m/s* and f in kHz, or equivalently,

$$\Delta f_{3dB}(\text{Hz}) = 1.76 h^{\frac{1}{2}} f \sin\theta \ , \tag{16b}$$

with h in m. In this model the frequency spectrum is broadened but unshifted.

Roderick[70] measured the forward scattered frequency distribution for $\theta = 10°$ at 20 kHz and 30 kHz, and at rms wave heights of 0.07 m and 0.24 m. The frequency distribution was found to be approximately Gaussian with no evident shift. Table I gives the 3 dB widths from these data and the corresponding values from Eq. (16b); the agreement is satisfactory. For the case with h = 0.07 m, the measured surface wave spectrum showed significant deviations from the Pierson-Moskowitz spectral form, and some differences from the predictions of Eq. (16) would be expected from this alone.

Table I. Comparison of Experimental and Model Spectral Widths

f (kHz)	h (m)	Experimental[a] 3 dB Width (Hz)	Model[b] 3 dB Width (Hz)
20	0.07	1.1	1.6
20	0.24	2.7	3.0
30	0.07	1.4	2.4
30	0.24	3.7	4.5

[a] From Ref. 70.

[b] From Eq. (16b).

* For direct use of the Pierson-Moskowitz surface wave spectrum, the wind speed should be measured at a height of 19.5 m.[16] However, use of wind speeds at the standard height of 10 m for U in Eq. (16a) should be sufficiently accurate. Wind speed normalization to a standard height is discussed in Ref. 69.

Eq. (16) has not been experimentally verified over a broad range of conditions at high frequencies – in particular, not at very low grazing angles where Eq. (16) is known to be unreliable.[65] The reasons for uncertainty are the same as mentioned in Section IV: shadowing, multiple scattering, and the breakdown of the Kirchhoff approximation at low grazing angles. Until such time as better information exists for very low grazing angles, we recommend as an alternate model substituting the effective rms surface slope angle, γ_0, for θ in Eq. (16) when $\theta < \gamma_0$. Some motivation of this choice is given in Section V.B. The slope angle γ_0 is given by Eq. (7).

Our recommendation for forward scattering frequency broadening is to assume an unshifted Gaussian spectral form for all wind speeds, since conditions of low roughness ($\chi \lesssim 1$) are relatively rare at high acoustic frequencies. The 3 dB spectral width is given by Eq. (16), but the alternate model at low grazing angles as noted above is suggested as a bound on the uncertainty.

At high sea states the effects of near surface bubbles must be taken into account as discussed earlier. The dominant effect on forward scattering will be attenuation, but scattering from bubbles will also occur and this process may affect the *frequency spectrum* when the attenuation is high. McDaniel and Gorman[71] have recently considered the effect of bubbles on the backscattered frequency spectrum, but the forward scattering problem has yet to be treated. No quantitative estimate of this effect is presently available.

VIII. STATISTICS

Several investigators have shown that when the roughness is large ($\chi \gtrsim 2$) the amplitude statistics over an ensemble of pings after a forward bounce are described to a reasonable approximation by a Rayleigh distribution.[12,14,72-74] For low roughness ($\chi \lesssim 2$), the constant reflected component plus a random scattered component has been modeled with the Rician distribution.[12,75,76] Since the low roughness condition seldom occurs at high frequencies, and since the Rician distribution is more concentrated about the mean* than the Rayleigh distribution, we recommend use of the Rayleigh distribution. Thus, the relative probability of obtaining a pressure amplitude (or envelope value), A, is given by[77]

$$P(A) = \frac{A}{<p^2>} \exp\left[-A^2/2<p^2>\right] , \tag{17a}$$

where p is the instantaneous pressure and $< >$ denotes ensemble average at a given time in the ping cycle. The mean square instantaneous pressure $<p^2> = \frac{1}{2}<A^2>$. The equivalent intensity distribution is

$$P(I) = \frac{1}{<I>} \exp\left[-I/<I>\right] , \tag{17b}$$

where I is proportional to A^2. It should be understood that the models in Section V pertain to the mean $<I>$.

* The point is that the Rayleigh distribution gives a greater probability of large deviations from the mean, and presumably it is the more conservative choice to assume a Rayleigh distribution for all conditions.

APPENDIX A

A FORWARD SCATTERING MODEL IN THE HIGH FREQUENCY LIMIT

A simplified model for forward scattering strengths can be obtained in the high frequency limit, i.e., by letting $\lambda \to 0$. For a Gaussian, isotropic distribution of surface slopes, the scattering strength can be written[2,78,79]

$$S_S = 10 \log \left[\frac{\sec^4 \gamma}{4\pi s^2} \exp \left[- \frac{\tan^2 \gamma}{s^2} \right] \right] , \qquad \text{(A1)}$$

where $\tan \gamma$ is the necessary surface slope at the local scattering region that would "reflect" a ray from the transmitter to the receiver. The mean square surface slope* is given by

$$s^2 = < \left[\frac{\partial \xi}{\partial x} \right]^2 + \left[\frac{\partial \xi}{\partial y} \right]^2 > \equiv \tan^2 \gamma_0 ,$$

where ξ (x,y) represents the surface height and where x and y are orthogonal coordinates in the plane of the mean surface; the angle γ_0 is the rms slope angle.

To estimate s^2 we use the results of optical glitter measurements of ocean surface slopes made by Cox and Munk[80,81] and conveniently presented by Phillips.[82] We expect the high surface wave numbers to have little effect, because of the finite acoustic wavelength, and therefore not contribute to the effective rms slope.[83-85] This is crudely accounted for here by using the slope distribution measured with surface oil slicks, which eliminated surface wavelengths shorter than ~ 30 cm. The same approximation has been found useful in modeling electromagnetic scattering from the ocean surface.[86] From Ref. 82 we then obtain for wind speed U in m/s at a

* Care is necessary here since some authors define s^2 to be the mean square slope for one direction only. In this case, s^2 in Eq. (A1) and Eq. (A2) is replaced by $2s^2 = 2 \tan^2 \gamma_0$.

10 m height

$$s^2 = 4.6 \times 10^{-3} \ln\ (2.1U^2)\ , \qquad \text{(A2)}$$

for $U > 1$ m/s. From Eq. (A2) it can be readily shown that the rms slope angle saturates at about 8° for $U \gtrsim 5$ m/s (see also Figure 4.23 in Ref. 82). Thus $\gamma_0 \cong 8°$ is an estimate for an effective rms surface slope for typical ocean conditions.

In Figure A-1, the scattering strength model given by Eq. (A1) and Eq. (A2) is compared with forward scattering data obtained by APL.[43] Since for these data the scattering was in-plane, i.e., the scattering region was in the vertical plane containing the transmitter and a highly directional receiver, the slope angle is given simply by $\gamma = \dfrac{\theta_s - \theta_i}{2}$, where θ_s and θ_i are the scattered and incident grazing angles, respectively. For specular scattering, $\gamma = 0$.

The approximate agreement between experiment and model in Figure A-1 (and other similar comparisons, including APL vertical incidence data[43]) supports the use of the high frequency limit for making estimates of forward scattering properties.

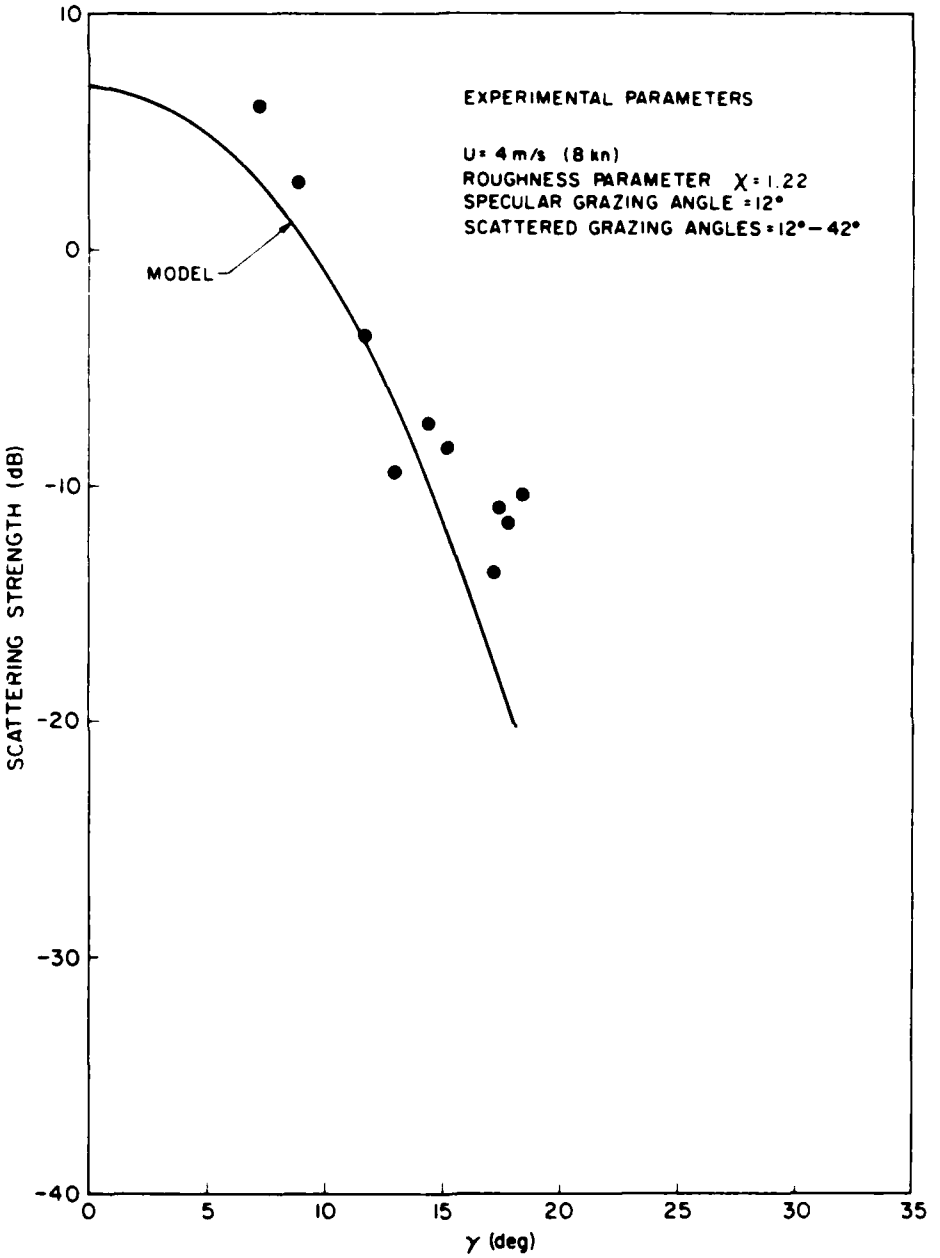

Figure A-1. Measured in-plane surface forward scattering strengths at low wind speed compared with model based on the high frequency limit. The surface slope angle γ is zero for scattering in the specular direction.

APPENDIX B

A BUBBLE LOSS MODEL

Suppose an incident plane wave of intensity, I_i, interacts with a surface with incident and outgoing grazing angles equal to θ. Resonant bubbles, assumed here to be homogeneous in the horizontal plane, will by themselves reduce the final intensity, I_f, to

$$I_f = I_i \exp\left[- \frac{2}{\sin\theta} \int_d^\infty S_e(z)dz \right] , \tag{B1}$$

where S_e is the total extinction cross section per unit volume (absorption plus scattering). Obviously, near surface bubbles are not just dependent on the depth, z, but sufficient information is not available to model the horizontal structure. Note that in Eq. (B1), the acoustic path is integrated up to a depth d below the surface, and not to the mean surface ($d = 0$). For high bubble attenuation, some account should be made for scattering from wave troughs, which extend down from the mean surface. This will be done later (very approximately) by choosing a $d > 0$.

We define a surface bubble loss (SBL) to be

$$\text{SBL(dB)} = 10 \log \frac{I_i}{I_f} = -10 \log \alpha_b$$

(see Eq. (2)), and Eq. (B1) yields

$$\text{SBL} = \frac{8.686}{\sin\theta} \int_d^\infty S_e(z)dz \ . \tag{B2}$$

The total extinction cross section per unit volume is given by[52]

$$S_e(z) = 1.7 \times 2\pi^2 a_R^3 \left. \frac{dn}{da} \right|^{a_R} / \delta_R \ . \tag{B3}$$

The factor 1.7 is given by Medwin[52] to account for nonresonant contributions to absorption and scattering. The radius of resonant bubbles a_R in μm at depth z in m is related to frequency f in kHz by

$$a_R = 3.25 \times 10^3 (1 + 0.1z)^{\frac{1}{2}} / f \quad . \tag{B4}$$

The quantity $\left.\frac{dn}{da}\right|^{a_R}$ is the number of bubbles per unit volume per unit bubble radius evaluated at the radius a_R, and is discussed below. The damping constant δ_R is given by

$$\delta_R = 0.0136(1 + 0.1z) \quad . \tag{B5}$$

Until better information is available, we will estimate the bubble distribution from the data of Johnson and Cooke[48] and Kolovayev[49] in a form similar to that used by Novorini and Bruno.[45] Thus,

$$\frac{dn}{da} = S_0 a^{-p} \left[\frac{U}{3}\right]^q e^{-z/L} \quad , \tag{B6}$$

with bubble radius a in μm. Below a wind speed U of about 3 m/s, bubble generation would not be expected at all,[87] but for $U \lesssim 3$ m/s the SBL derived here is insignificant.

Johnson and Cooke data imply $p = 5$* for

$$\begin{cases} 68\ \mu m \lesssim a \lesssim 136\ \mu m \\ 24\ \text{kHz} \lesssim f \lesssim 48\ \text{kHz} \end{cases} ,$$

where here (and in what follows) the frequency range is the range of resonant frequencies that corresponds to the range of bubble radii. In the Johnson and Cooke

* This is outside the range for which Medwin's factor of 1.7 in Eq. (B3) is thought to be valid. This point deserves further investigation.

data there is an indication of smaller p for $a > 136\,\mu m$ ($f < 24$ kHz). Kolovayev, with more data on larger bubbles, finds $p = 3.5$ for

$$\begin{cases} 115\,\mu m \lesssim a \lesssim 350\,\mu m \\ 9\text{ kHz} \lesssim f \lesssim 28\text{ kHz} \end{cases}$$

In Eq. (B6) we choose

$$p = \begin{cases} 5 & 68\,\mu m \leqq a \leqq 136\,\mu m\,(24\text{ kHz} \leqq f \leqq 48\text{ kHz}) \\ 3.5 & 136\,\mu m \leqq a \leqq 280\,\mu m\,(15\text{ kHz} \leqq f \leqq 24\text{ kHz}) \end{cases}.$$

Next, following Wu,[46] we take in Eq. (B6) $q = 4.5$, which gives the dependence of the bubble density on wind speed. This dependence is not well determined experimentally.

The exponential depth dependence of the bubble density (to at least a 3 m depth) is consistent with the data of Johnson and Cooke,[48] Kolovayev,[49] and Thorpe.[47] For the Johnson and Cooke data, $L \cong 1$ m for $U \cong 12$ m/s. We assume L is proportional to the waveheight. Using the fact that for a Pierson–Moskowitz surface wave spectrum the waveheight scales with U^2, we obtain

$$L = (U/12)^2\ , \tag{B7}$$

with L in m. With these choices in Eq. (B6) and using the data of Johnson and Cooke, we find $S_0 = 2.6 \times 10^{10}\text{m}^{-3}\mu\text{m}^{-1}$ for $p = 5$, and $S_0 = 1.6 \times 10^{7}\text{m}^{-3}\mu\text{m}^{-1}$ for $p = 3.5$.*

We choose d in Eq. (B2) to be given by L to account roughly for the presence of wave troughs. With this choice d is about 1.4 times the rms waveheight (h), but still less than half the significant waveheight of about $4h$ (peak-to-trough). Such a normalization should clearly be done by comparison with data, but the required data base is lacking.

---

* The wind speeds for the Johnson and Cooke data were not measured at the standard height of 10 m, and to be rigorous, wind speed normalization to 10 m should be made (see Ref. 69). However, very preliminary comparisons with new APL data (4/83) appear to support Eq. (15) as is, taking U to be the wind speed at 10 m.

With the rapid decrease in bubble density with depth implied by Eq. (B6) and Eq. (B7), the factor $(1 + 0.1z)$ can be set to 1 in Eq. (B4) and Eq. (B5). Finally, combining Eqs. (B2)-(B7) and doing the elementary integration over z gives Eq. (15).

Scattering from bubbles will effectively place a limit on the absorption loss, and this limit can be estimated from the scattering properties of bubbles. In this limit, the bubble density is so high that the surface is completely screened from the incident pulse. The effective surface scattering strength from bubbles near the specular direction would be estimated from Figure 4, Section VI, at about -30 dB, similar to backscattering levels at about the same grazing angles.[69] Thus, the scattering differential cross section per unit area of the surface (see Section II) is roughly a constant at about $\sigma \cong 10^{-3}$. The fraction F of the incident energy scattered into the solid angle Ω about the specular direction is given by

$$F = \sigma\Omega / \sin\theta \ , \tag{B8}$$

where θ is the specular grazing angle. If we associate with the bounce path the scattered energy within a cone of half angle α of the specular ray, then $\Omega = 2\pi\,(1 - \cos\alpha)$. Considering the discussion in Section V.A, it would appear reasonable to choose the full angle $2\alpha \cong 20°$, or $\alpha = 10°$. However, the actual beam widths and pulse length for a particular application should be taken into account in making such an estimate. The maximum bounce loss is then given by $\mathrm{SBL}_{\max}(\mathrm{dB}) = -10 \log F$. With the typical value of $\theta = 10°$, we find $\mathrm{SBL}_{\max} \cong 33$ dB.

Alternately, a theoretical estimate can be made from the work of McDaniel and Gorman.[69] From Eq. (15)* of Ref. 69 we have in the limit of large bubble densities

$$\sigma = \frac{1}{8\pi}\frac{\delta_R}{\delta}\sin\theta \ , \tag{B9}$$

---

* A typographical error in Eq. (15) of Ref. 69 has been corrected (see Ref. 88), which reduces the result by π^2. Also, inclusion of Medwin's factor[52] of 1.7 in attenuation [Eq. (10), Ref. 69] as well as in scattering [Eq. (8), Ref. 69] yields an additional reduction by a factor of 1.7. Eq. (B9) can also be written $\sigma = \frac{1}{8\pi}\frac{S_s}{S_e}\sin\theta$, where S_s and S_e are the total scattering and extinction cross sections. The cross section notation here follows Ref. 52 and differs from Ref. 69.

where the damping factor δ depends weakly on the bubble radius.[89] Note that with the use of Eq. (B9) in Eq. (B8), the sin θ factor cancels. With the use of the typical value[89] $\delta = 0.07$ and with the same Ω as before, Eq. (B8) and Eq. (B9) lead to $SBL_{max} \cong 31$ dB.

Thus, we adopt the estimate $SBL_{max} = 30$ dB.

REFERENCES

1. A. Ishimaru, *Wave Propagation and Scattering in Random Media* (Academic Press, New York, 1978) Vol. I, pp. 77-80, and Vol. II, Ch. 21.

2. C. Eckart, "The Scattering of Sound from the Sea Surface," J. Acoust. Soc. Am. **25**, 566-570 (1953).

3. C.S. Clay, "Coherent Reflection of Sound from the Ocean Bottom," J. Geophys. Res. **71**, 2037-2046 (1966).

4. M.L. Boyd and R.L. Deavenport, "Forward and Specular Scattering from a Rough Surface: Theory and Experiment," J. Acoust. Soc. Am. **53**, 791-801 (1973).

5. R.K. Moore and B.E. Parkins, "Omnidirectional Scattering of Acoustic Waves from Rough Surfaces of Known Statistics," J. Acoust. Soc. Am. **40**, 170-175 (1966).

6. W.D. Boles, A.K. Fung, and R.K. Moore, "Bistatic Measurements of Acoustic Waves Scattered from a Statistically Rough Known Surface," J. Acoust. Soc. Am. **45**, 1040-1044 (1969).

7. E.P. Gulin, "Amplitude and Phase Fluctuations of a Sound Wave Reflected from a Statistically Uneven Surface," Sov. Phys. Acoust. **8**, 135-140 (1962).

8. D.R. Melton and C.W. Horton, Sr., "Importance of the Fresnel Correction in Scattering from a Rough Surface. I. Phase and Amplitude Fluctuations," J. Acoust. Soc. Am. **47**, 290-298 (1970).

9. J.F. McDonald and R.C. Spindel, "Implications of Fresnel Corrections in a Non-Gaussian Surface Scatter Channel," J. Acoust. Soc. Am. **50**, 746-757 (1971).

10. L. Fortuin, "The Sea Surface as a Random Filter for Underwater Sound Waves," J. Acoust. Soc. Am. **52**, 302-315 (1972).

11. F.B. Tuteur and J.F. McDonald, "Scattering Function for Multiple-Bounce Underwater Acoustic Channels," J. Acoust. Soc. Am. **64**, 614-621 (1978).

12. E.P. Gulin and K.I. Malyshev, "Statistical Characteristics of Sound Signals Reflected from the Undulating Sea Surface," Sov. Phys. Acoust. **8**, 228-234 (1963).

13. J.C. Beckerle, "Effects of Ocean Waves on Acoustic Signals to Very Deep Hydrophones," J. Acoust. Soc. Am. **35**, 267-272 (1963).

14. D.C. Whitmarsh, "Underwater-Acoustic-Transmission Measurements," J. Acoust. Soc. Am. **35**, 2014-2018 (1963).

15. See, for example, P. Beckmann and A. Spizzichino, *The Scattering of Electromagnetic Waves from Rough Surfaces* (Pergamon Press, Oxford, 1963), Ch. 5.

16. W.J. Pierson, Jr. and L. Moskowitz, "A Proposed Spectral Form for Fully Developed Wind Seas Based on the Similarity Theory of S.A. Kitaigorodskii," J. Geophys. Res. **69**, 5181-5190 (1964).

17. W.J. Pierson, "The Spectral Ocean Wave Model (SOWM), A Northern Hemisphere Computer Model For Specifying and Forecasting Ocean Wave Spectra," DTNSRDC-82/011, David W. Taylor Naval Ship Research and Development Center, Bethesda, MD (1982).

18. J.M. Proud, Jr., R.T. Beyer, and P. Tamarkin, "Reflection of Sound from Randomly Rough Surfaces," J. of Appl. Phys. **31**, 290-299 (1960).

19. H. Medwin, "Specular Scattering of Underwater Sound from a Wind Driven Surface," J. Acoust. Soc. Am. **41**, 1485-1495 (1967).

20. C.S. Clay, H. Medwin, and W.M. Wright, "Specularly Scattered Sound and the Probability Density Function of a Rough Surface," J. Acoust. Soc. Am. **53**, 1677-1682 (1973).

21. J.G. Zornig and J.F. McDonald, "Direct Measurement of Surface-Scatter Channel Coherence by Impulse Probing," J. Acoust. Soc. Am. **55**, 1205-1211 (1974).

22. H. Medwin and C.S. Clay, "Dependence of Spatial and Temporal Correlation of Forward-Scattered Underwater Sound on the Surface Statistics II. Experiment," J. Acoust. Soc. Am. **47**, 1419-1429 (1970).

23. B.E. Parkins, "Scattering from the Time-Varying Surface of the Ocean," J. Acoust. Soc. Am. **42**, 1262-1267 (1967).

24. P.J. Lynch, "Curvature Corrections to Rough-Surface Scattering at High Frequencies," J. Acoust. Soc. Am. **47**, 804-815 (1970).

25. E.G. Liszka and J.J. McCoy, "Scattering at a Rough Boundary--Extensions of the Kirchhoff Approximations," J. Acoust. Soc. Am. **71**, 1093-1100 (1982).

26. S.O. Rice, "Reflection of Electromagnetic Waves from Slightly Rough Surfaces," Comm. Pure Appl. Math. **4**, 351-378 (1951).

27. H.W. Marsh, M. Schulkin, and S.G. Kneale, "Scattering of Underwater Sound by the Sea Surface," J. Acoust. Soc. Am. **33**, 334-340 (1961).

28. W. Bachmann, "A Theoretical Model for the Backscattering Strength of a Composite-Roughness Sea Surface, J. Acoust. Soc. Am. **54**, 712-716 (1973).

29. E.Y. Harper and F.M. Labianca, "Perturbation Theory for Scattering of Sound From a Point Source by a Moving Rough Surface in the Presence of Refraction," J. Acoust. Soc. Am. **57**, 1044-1051 (1975).

30. E.Y. Harper and F.M. Labianca, "Scattering of Sound From a Point Source by a Rough Surface Progressing Over an Isovelocity Ocean," J. Acoust. Soc. Am. **58**, 349-364 (1975).

31. W.A. Kuperman, "Coherent Component of Specular Reflection and Transmission at a Randomly Rough Two-Fluid Interface," J. Acoust. Soc. Am. **58**, 365-370 (1975).

32. S.O. McConnell and E.I. Thorsos, "Acoustic Characterization of the Shallow Water Quinault Range (U)," APL-UW 8205, Applied Physics Laboratory, University of Washington, 1982 (Confidential). (See Section IV.A and Figure 36.)

33. S.O. McConnell, APL-UW (personal communication on unpublished data).

34. R.H. Nichols and A. Senko, "Amplitude Fluctuations of Low-Frequency Underwater Acoustic Pulses Reflected from the Ocean Surface," J. Acoust. Soc. Am. **55**, 550-554 (1974).

35. R.H. Adlington, "Acoustic-Reflection Losses at the Sea Surface, Measured with Explosive Sources," J. Acoust. Soc. Am. **35**, 1834-1835 (1963).

36. K.Y. Moravan, "Analysis of Reverberation Data from Fixed and Moving Platforms and Comparison with Simulations (U)," APL-UW 8106, Applied Physics Laboratory, University of Washington, 1982. (Confidential)

37. D.W. Princehouse, APL-UW (personal communication).

38. H.W. Marsh and M. Schulkin, "Shallow-Water Transmission," J. Acoust. Soc. Am. **34**, 863-864 (1962).

39. J.F. McDonald and F.B. Tuteur, "Calculation of the Range-Doppler Plot for a Doubly Spread Surface-Scatter Channel at High Rayleigh Parameters," J. Acoust. Soc. Am. **57**, 1025-1029 (1975).

40. J.F. McDonald, F.B. Tuteur, and J.G. Zornig, "Spatial Interfrequency Correlation Effects in a Surface-Scatter Channel," J. Acoust. Soc. Am. **59**, 1284-1293 (1976).

41. F.B. Tuteur, "Underwater Acoustic Scatter Channels with Several Bounces," J. Acoust. Soc. Am. **60**, 840-843 (1976).

42. I.S. Gradshteyn and I.M. Ryzhik, *Tables of Integrals, Series, and Products* (Academic Press, New York, 1980), p. 930.

43. S.O. McConnell, "Surface Forward Reflection and Scattering, Surface Backscattering, and Ambient Noise Measurements Made During GTV Adaptive Signal Processing Test (U)," APL-UW TM 5-83, Applied Physics Laboratory, University of Washington, 1983. (Confidential)

44. M. Schulkin, "Surface-Coupled Losses in Surface Sound Channel Propagation. II," J. Acoust. Soc. Am. **45**, 1054-1055(L) (1969).

45. J.C. Novarini and D.R. Bruno, "Effects of the Sub-Surface Bubble Layer on Sound Propagation," J. Acoust. Soc. Am. **72**, 510-514 (1982).

46. J. Wu, "Bubble Populations and Spectra in Near-Surface Ocean: Summary and Review of Field Measurements," J. Geophys. Res. **86**, 457-463 (1981).

47. S.A. Thorpe, "On the Clouds of Bubbles Formed by Breaking Wind-Waves in Deep Water, and Their Role in Air-Sea Gas Transfer," Phil. Trans. R. Soc. Lond. A **304**, 155-210 (1982).

48. B.D. Johnson and R.C. Cooke, "Bubble Populations and Spectra in Coastal Waters: A Photographic Approach," J. Geophys. Res. **84**, 3761-3766 (1979).

49. D.A. Kolovayev, "Investigation of the Concentration and Statistical Size Distribution of Wind-Produced Bubbles in the Near-Surface Ocean," Oceanology (Engl. transl.) **15**, 659-661 (1976).

50. M. Schulkin, APL-UW (personal communication).

51. H. Medwin, "In Situ Acoustic Measurements of Bubble Populations in Coastal Ocean Waters," J. Geophys. Res. **75**, 599-611 (1970).

52. H. Medwin, "In Situ Acoustic Measurements of Microbubbles at Sea," J. Geophys. Res. **82**, 971-976 (1977).

53. W.I. Roderick and B.J. Cron, "Frequency Spectra of Forward-Scattered Sound from the Ocean Surface," J. Acoust. Soc. Am. **48**, 759-766 (1970).

54. M.V. Brown and G.V. Frisk, "Frequency Smearing of Sound Forward-Scattered from the Ocean Surface," J. Acoust. Soc. Am. **55**, 744-749 (1974).

55. H.A. DeFerrari and Lan Nghiem-Phu, "Scattering Function Measurements for a 7-NM Propagation Range in the Florida Straits," J. Acoust. Soc. Am. **56**, 47-52 (1974).

56. V.I. Neklyudov and S.D. Chuprov, "Experimental Study of the Amplitude Fluctuation Spectra of Tone-Burst Signals Reflected from the Ocean Surface for Large Values of the Rayleigh Parameter," Sov. Phys. Acoust. **22**, 43-45 (1976).

57. J.A. Shooter and S.K. Mitchell, "Observations of Acoustic Sidebands in CW Tones Received at Long Ranges," J. Acoust. Soc. Am. **60**, 829-832 (1976).

58. D.J. Ramsdale, "Acoustic Sidebands from CW Sources Towed at Long Range in the Deep Ocean," J. Acoust. Soc. Am. **63**, 391-395 (1978).

59. C. Gazanhes, J. Leandre, and J.P. Lefebvre, "Spectral Structure of an Ultrasound Wave Scattered by a Random Surface: Application to the Scattering of Sound from the Sea Surface," J. Acoust. Soc. Am. **63**, 1347-1352 (1978).

60. J.G. Zornig, "Physical Model Studies of Forward Surface Scatter Frequency Spreading," J. Acoust. Soc. Am. **64**, 1492-1499 (1978).

61. B.E. Parkins, "Scattering from the Time-Varying Surface of the Ocean," J. Acoust. Soc. Am. **42**, 1262-1267 (1967).

62. B.E. Parkins, "Reflection and Scattering from a Time-Varying Rough Surface--The Nearly Complete Lloyd's Mirror Effect," J. Acoust. Soc. Am. **49**, 1484-1490 (1971).

63. J.F. McDonald and P.M. Schultheiss, "Asymptotic Frequency Spread in Surface-Scatter Channels at Large Rayleigh Numbers," J. Acoust. Soc. Am. **57**, 160-164 (1975).

64. E.Y. Harper and F.M. Labianca, "Scattering of Sound from a Point Source by a Rough Surface Progressing Over an Isovelocity Ocean," J. Acoust. Soc. Am. **58**, 349-364 (1975); J. Acoust. Soc. Am. **59**, 484 (1976).

65. R.L. Swarts and C.J. Eggen, "Simplified Model of the Spectral Characterization of High-Frequency Surface Scatter," J. Acoust. Soc. Am. **59**, 846-851 (1976).

66. S.D. Chuprov, "Relationship Between the Spectrum of a Signal Reflected from a Rough Sea Surface and the Sea-Wave Spectrum in the Case of Small Roughness," Sov. Phys. Acoust. **24**, 62-67 (1978).

67. J. Preston and R. Nisley, "Simple Frequency Modulation Model for Surface Reflection of a CW Tow," J. Acoust. Soc. Am. **64**, 601-604 (1978).

68. F.B. Tuteur, H. Tung, and J.G. Zornig, "Asymmetric Doppler Amplitudes in the Surface Scatter Channel for Crosswind Transmitter-Receiver Geometry," J. Acoust. Soc. Am. **68**, 1184-1192 (1980).

69. S.T. McDaniel and A.D. Gorman, "Acoustic and Radar Sea Surface Backscatter," J. Geophys. Res. **87**, 4127-4136 (1982).

70. W.I. Roderick and W.G. Kanabis, "Scattering Coefficients and Doppler Spectra of Specularly Scattered Sound from the Sea Surface," J. Acoust. Soc. Am. Suppl. 1 **69**, S96 (1981).

71. S.T. McDaniel and A.D. Gorman, "Spectral Spread of Sea-Surface Reverberation," J. Acoust. Soc. Am. **74**, 241-248 (1983).

72. M.J. Pollak, "Surface Reflection of Sound at 100 kc," J. Acoust. Soc. Am. **30**, 343-347 (1958).

73. G.E. Smirnov and O.S. Tonakanov, "Fluctuations in Hydroacoustic Pulse Signals on Reflection from a Water Surface on which Waves are Present," Sov. Phys. Acoust. **6**, 480-487 (1961).

74. O.S. Tonakanov, "Sound Fluctuations in Double Reflections from an Undulating Water Surface," Sov. Phys. Acoust. **10**, 211-212 (1964).

75. V.V. Borodin and E.A. Kopyl, "Unreliability of Coherence Estimates Based on the Amplitudes of Signals Reradiated by a Sea Surface," Sov. Phys. Acoust. **25**, 445-446 (1979).

76. See Ref. 15, Ch. 7.

77. B.F. Cron and W.R. Schumacher, "Theoretical and Experimental Study of Underwater Sound Reverberation," J. Acoust. Soc. Am. **33**, 881-888 (1961).

78. D.E. Barrick, "Rough Surface Scattering Based on the Specular Point Theory," IEEE Trans. Antennas and Propagation **AP-16**, 449-454 (1968).

79. D.E. Barrick and W.H. Peak, "Scattering from Surfaces with Different Roughness Scales: Analysis and Interpretation," BAT-197A-10-3, Battelle Memorial Institute, Columbus Laboratories, 1967.

80. C.S. Cox and W.H. Munk, "Statistics of the Sea Surface Derived from Sun Glitter," J. Mar. Res. **13**, 198-227 (1954).

81. C.S. Cox and W.H. Munk, "Measurements of the Roughness of the Sea Surface from Photographs of the Sun's Glitter," J. Optical Soc. Am. **44**, 838-850 (1954).

82. O.M. Phillips, *The Dynamics of the Upper Ocean* (Cambridge University Press, Cambridge, 1977), pp. 177-179.

83. T. Hagfors, "Relationship of Geometric Optics and Autocorrelation Approaches to the Analysis of Lunar and Planetary Radar," J. Geophys. Res. **71**, 379-383 (1966).

84. P.J. Lynch, "Curvature Corrections to Rough-Surface Scattering at High Frequencies," J. Acoust. Soc. Am. **47**, 804-815 (1970).

85. G. Yu. Narodnitskiy, "On Radiation Wavelength Considerations in Calculations of the Energy Characteristics of Scattering by the Sea Surface," Izvestiya, Atmospheric and Oceanic Physics **15**, 856-858 (1979).

86. G.R. Valenzuela, "Theories for the Interaction of Electromagnetic and Oceanic Waves--A Review," Boundary Layer Meteorology **13**, 61-85 (1978).

87. S.A. Thorpe and P.N. Humphries, "Bubbles and Breaking Waves," Nature **283**, 463-465 (1980).

88. S.T. McDaniel and A.D. Gorman, "Analysis of Acoustic and Radar Sea-Surface Reverberation Using the Composite-Roughness Model," Technical Memorandum, File No. TM 81-106, Applied Research Laboratories, The Pennsylvania State University, 1981.

89. R.J. Urick, *Principles of Underwater Sound* (McGraw-Hill, New York, 1975) p. 226.

UNCLASSIFIED

SECURITY CLASSIFICATION OF THIS PAGE (When Data Entered)

REPORT DOCUMENTATION PAGE

READ INSTRUCTIONS BEFORE COMPLETING FORM

1 REPORT NUMBER: APL-UW 7-83	2 GOVT ACCESSION NO.: AD-A150 115
3 RECIPIENT'S CATALOG NUMBER:	
4 TITLE (and Subtitle): SURFACE FORWARD SCATTERING AND REFLECTION	5 TYPE OF REPORT & PERIOD COVERED: Technical
	6 PERFORMING ORG. REPORT NUMBER:
7 AUTHOR(s): E. I. Thorsos	8 CONTRACT OR GRANT NUMBER(s): N00024-81-C-6042
9 PERFORMING ORGANIZATION NAME AND ADDRESS: Applied Physics Laboratory, University of Washington, 1013 N.E. 40th St., Seattle, WA 98105	10 PROGRAM ELEMENT, PROJECT, TASK AREA & WORK UNIT NUMBERS: P.E. 62759N
11 CONTROLLING OFFICE NAME AND ADDRESS: Commander, Naval Sea Systems Command, Department of the Navy, Washington, D.C. 20362, Attn: Code 63R	12 REPORT DATE: May 1984 13 NUMBER OF PAGES: 41
14 MONITORING AGENCY NAME & ADDRESS (if different from Controlling Office): Naval Ocean Research & Development Activity (NORDA), Attn: NORDA Liaison Office (Code 113), 800 N. Quincy St. BT #1, Arlington, VA 22217	15 SECURITY CLASS. (of this report): Unclassified 15a DECLASSIFICATION DOWNGRADING SCHEDULE: N/A

16 DISTRIBUTION STATEMENT (of this Report)

Distribution limited to Department of Defense agencies only (Test and Evaluation). Other requests for this document should be referred to the Naval Sea Systems Command, Code 63R1.

17 DISTRIBUTION STATEMENT (of the abstract entered in Block 20, if different from Report)

18 SUPPLEMENTARY NOTES

19 KEY WORDS (Continue on reverse side if necessary and identify by block number)

Surface forward scattering
Surface forward reflection
Pulse elongation
Propagation simulations
Bubble absorption
Frequency spreading
Specular scattering

20 ABSTRACT (Continue on reverse side if necessary and identify by block number)

This report discusses high frequency (15-60 kHz) models of surface forward scattering and reflection that are appropriate for use in acoustic simulations based on ray tracing techniques. These models include the following properties of a pulse after a single surface interaction: (1) the amplitude as a function of time in or near the specular direction (which gives pulse (cont.)

DD FORM 1 JAN 73 1473 EDITION OF 1 NOV 65 IS OBSOLETE
S/N 0102 LF 014 6601

UNCLASSIFIED

SECURITY CLASSIFICATION OF THIS PAGE (When Data Entered)

20, cont.

elongation), (2) the corresponding amplitude statistics, (3) the partitioning into scattered (incoherent) and reflected (coherent) components in the specular direction, (4) the changes in the frequency spectrum due to the moving surface, and (5), at a simpler level, an effective reflection loss, e.g., for reverberation or one-way propagation simulations. Important absorption effects of near-surface bubbles due to breaking waves are also taken into account. It is assumed that the primary interest for simulations lies in representing the scattered signal by an effective reflection loss because of the difficulty of including forward scattering in simulations. Thus, a detailed description of the angular distribution of the scattered intensity near the specular direction is not given.

Because of the present lack of comprehensive experimental studies of surface forward scattering at high frequencies, these models are based primarily on heuristic arguments, theoretical studies, the use of experimental results at lower frequencies, and the use of laboratory experiments often at even higher frequencies.

END

FILMED

3-85

DTIC